Modeling and Control of Minimal Flow Unit Turbulence in Plane Couette Flow

Troy R. Smith
Dept. of Mechanical and Aerospace Engineering
Princeton University
Princeton, NJ 08544 USA
trsmith@math.princeton.edu

Jeff Moehlis
Prog. in Applied and Comp. Mathematics
Princeton University
Princeton, NJ 08544 USA
jmoehlis@math.princeton.edu

Philip J. Holmes
Dept. of Mechanical and Aerospace Engineering & Prog. in Applied and Comp. Mathematics
Princeton University
Princeton, NJ 08544 USA
pholmes@math.princeton.edu

Abstract

We model turbulent plane Couette flow for a Minimal Flow Unit (the smallest domain in which turbulence can be sustained) by expanding the velocity field as a sum of optimal modes calculated via the proper orthogonal decomposition from numerical data. Ordinary differential equations are obtained by Galerkin projection of the Navier-Stokes equations onto these modes. We consider a 6 mode (11-dimensional) model. When losses to neglected modes are ignored, the model captures some aspects of the turbulent state very well, but fails to accurately reproduce the velocity field dynamics. However, when energy-transfer to neglected modes is included, there is strong agreement with results from direct numerical simulations. This model provides empirical evidence that the "backbone" for Minimal Flow Unit turbulence is a periodic orbit. We then calculate the phase response curve for this periodic orbit, which describes the phase-shift of the oscillation as a function of the phase of an impulsive perturbation to the mean flow. We see that, depending on its timing, such a perturbation can either advance or retard the time at which subsequent streak breakdowns occur. This suggests how streak breakdown can be controlled through appropriately timed perturbations.

1 Introduction

In plane Couette flow (PCF), fluid is sheared between two infinite parallel plates moving at speed U_0, in opposite directions $\pm\mathbf{e}_x$; see Figure 1.1. The x, y, z-directions are defined to be the streamwise, wall normal, and spanwise directions, respectively. We nondimensionalize lengths in units of $d/2$ where d is the gap between the plates, velocities in units of U_0, time in units of $(d/2)/U_0$, and pressure in units of $U_0^2\rho$ where ρ is the fluid density. Laminar flow is then given by $\mathbf{U}_0 = y\mathbf{e}_x$, $-1 \le y \le 1$. The laminar state is linearly stable for all Reynolds numbers $Re = \frac{U_0 d}{2\nu}$ [1], where ν is the kinematic viscosity; however, both experiments and simulations exhibit sustained turbulence for sufficiently high Re and/or perturbation amplitudes (see, e.g., [2]). Writing $\mathbf{u} = (u_1, u_2, u_3)$, $\mathbf{x} = (x, y, z)$, the evolution equation for the perturbation $(\mathbf{u}(\mathbf{x}, t), p(\mathbf{x}, t))$ to laminar flow is

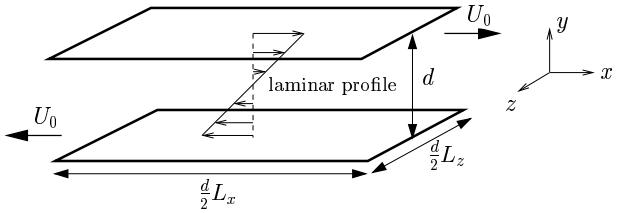

Figure 1.1: Geometry for plane Couette flow.

$$\frac{\partial}{\partial t}\mathbf{u} = -(\mathbf{u}\cdot\nabla)\mathbf{u} - y\frac{\partial}{\partial x}\mathbf{u} - u_2\mathbf{e}_x - \nabla p + \frac{1}{Re}\nabla^2\mathbf{u}. \quad (1.1)$$

The fluid is assumed to be incompressible, i.e.,

$$\nabla\cdot\mathbf{u} = 0, \quad (1.2)$$

and there are no-slip boundary conditions at the plates, i.e.,

$$\mathbf{u}|_{y=\pm1} = 0. \quad (1.3)$$

Finally, the flow is assumed periodic in the streamwise and spanwise directions, with lengths $L_x \equiv 1.75\pi$

and $L_z \equiv 1.2\pi$, respectively. This corresponds to the Minimal Flow Unit, the smallest domain in which turbulence can be sustained [3].

To model turbulent PCF, we perform a proper orthogonal decomposition (POD) on data from direct numerical simulations (DNS) of (1.1) at $Re = 400$. This identifies an energetically dominant set of empirical eigenmodes ("POD modes") from the data. We then construct models by Galerkin projection of (1.1) onto finite-dimensional subspaces spanned by the dominant modes, yielding ordinary differential equations for the evolution of the modal amplitudes; see [4] for details and references on this procedure, and [5] for an application to PCF turbulence at $Re = 400$ for a moderate aspect-ratio domain with $L_x = 4\pi$, $L_z = 2\pi$. (See also [6] for a similar approach to the study of MFU turbulence for channel flow, and, e.g., [7] and [8] for other low-dimensional models for shear flow turbulence.) Here we consider a 6 mode (11-dimensional) model which consists of a mode representing the spatial mean flow, two streamwise-invariant modes, one spanwise-invariant mode, and two "fully three-dimensional" modes. When energy-transfer to neglected modes is included, this model shows strong agreement with results from DNS. In particular, it provides empirical evidence that the "backbone" for Minimal Flow Unit turbulence is a periodic orbit. Consideration of this periodic orbit suggests how streak breakdown can be controlled through appropriately timed perturbations. We hope that this study of a "simple" turbulent flow in a simple geometry will stimulate the application of similar control ideas to delaying separation, reducing drag, and enhancing mixing in other turbulent flows.

2 Turbulence for The Minimal Flow Unit

The nature of the weakly turbulent flow in the Minimal Flow Unit was first described in [3]. Here the authors define the RMS modal velocity as

$$\mathrm{M}(n_x, n_z) = \left(\int_{-1}^{1} \left[\tilde{u}_1^2(n_x, y, n_z) + \tilde{u}_2^2(n_x, y, n_z) + \tilde{u}_3^2(n_x, y, n_z) \right] dy \right)^{1/2}, \quad (2.1)$$

where the tildes represent Fourier mode amplitudes, and they discuss the temporal behavior of this quantity for various wavenumber pairs (n_x, n_z). They find that the RMS modal velocity for several modes shows almost periodic behavior and, in particular, that $\mathrm{M}(0,1)$ and $\mathrm{M}(1,0)$ are roughly of opposite phase: a peak in the former is often accompanied by a trough in the latter, and vice versa, as illustrated in Fig. 2.1 (cf. Fig. 3(a) in [3]). This figure also shows that the temporal dynamics of $\mathrm{M}(1,1)$ is much the same as that of $\mathrm{M}(1,0)$, while $\mathrm{M}(0,2)$ does not display a great deal of regularity. A close-up of one representative "cycle" is shown

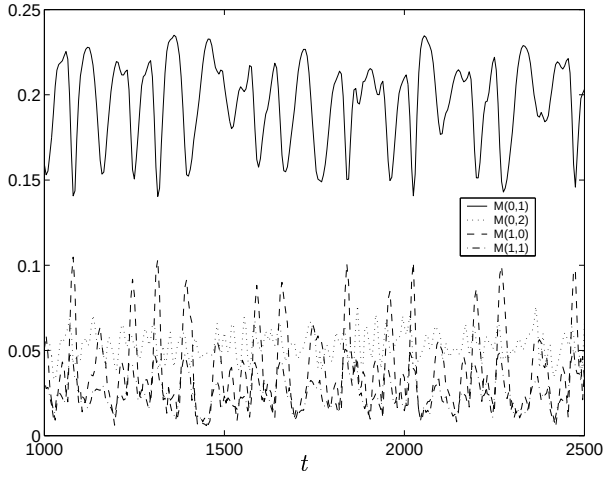

Figure 2.1: The behavior of the RMS modal velocities for several wavenumbers.

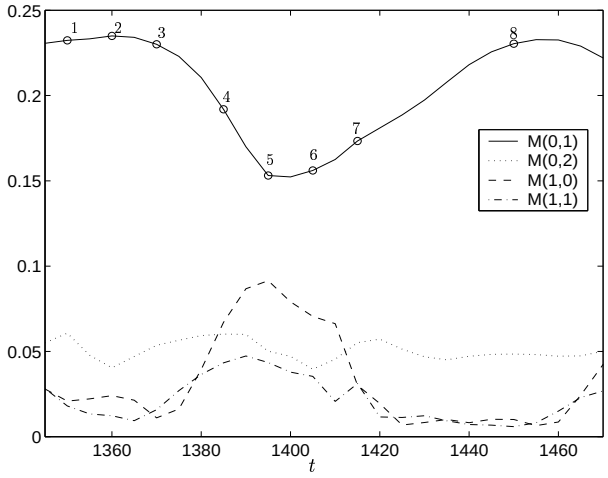

Figure 2.2: One representative cycle from Fig. 2.1.

in Fig. 2.2 (cf. Fig. 3(b) in [3]). Here the pertinent behavior is somewhat more clearly observed. Fig. 2.3 (cf. Fig. 2 in [3]) shows midplane contours of the streamwise velocity at the times labeled on the $\mathrm{M}(0,1)$ curve in Fig. 2.2. At the time labeled '1', the flow shows prominent streaks, that is, streamwise-coherent structures with variation of the streamwise velocity with respect to spanwise position. The streaks have broken down by the time labeled '5', then they regenerate and the process begins anew.

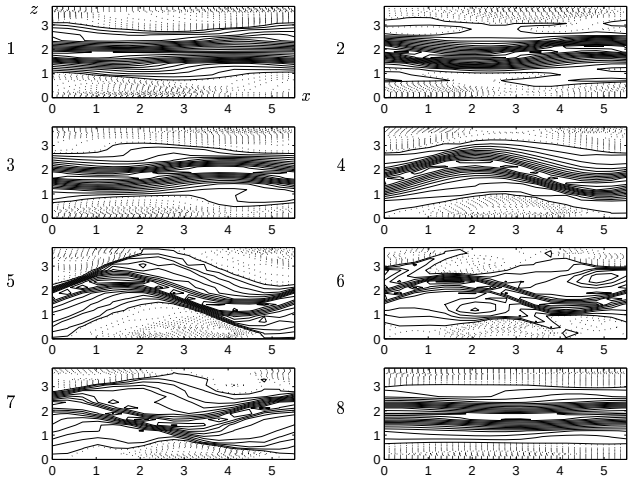

Figure 2.3: Midplane streamwise-velocity contours from the DNS.

3 The Proper Orthogonal Decomposition

Details of the POD procedure are described in Ref. [4]; here we summarize key aspects. The POD modes $\mathbf{\Phi} = (\Phi_1, \Phi_2, \Phi_3)$ are chosen to maximize the average projection of the perturbation $\mathbf{u} = (u_1, u_2, u_3)$ onto each mode. First, we define the inner product on the space of velocity fields $[L^2(\Omega)]^3$ as

$$(\mathbf{f}, \mathbf{g}) \equiv \sum_{j=1}^{3} \int\int\int_{\Omega} f_j(\mathbf{x}) g_j^*(\mathbf{x}) d^3\mathbf{x},$$

where the subscripts identify components of the functions and * denotes complex conjugation. The POD modes are chosen to maximize the average projection of the perturbation $\mathbf{u}$ onto each mode; specifically, we seek functions $\mathbf{\Phi}(\mathbf{x}) \in [L^2(\Omega)]^3$ such that the quantity $\langle |(\mathbf{u}, \mathbf{\Phi})|^2 \rangle / ||\mathbf{\Phi}||^2$ is maximized, where $||\cdot|| = (\cdot,\cdot)^{1/2}$ and $\langle\cdot\rangle$ is an (ensemble or time) averaging operation. This leads to the eigenvalue problem

$$\sum_{j=1}^{3} \int\int\int_{\Omega} \langle u_i(\mathbf{x},t) u_j^*(\mathbf{x}',t) \rangle \Phi^{(n)}_{j n_x n_z}(\mathbf{x}') d^3\mathbf{x}' = \lambda^{(n)}_{n_x n_z} \Phi^{(n)}_{i n_x n_z}(\mathbf{x}), \quad i = 1,2,3, \quad (3.1)$$

where the "quantum numbers" $n \in \mathbb{Z}^+$, and wavenumbers $n_x, n_z \in \mathbb{Z}$ distinguish different POD modes. The eigenvalue $\lambda^{(n)}_{n_x n_z}$ is twice the average kinetic energy in the POD mode $\mathbf{\Phi}^{(n)}_{n_x n_z}$. The (orthogonal) POD modes are normalized so that

$$(\mathbf{\Phi}^{(n)}_{n_x n_z}, \mathbf{\Phi}^{(n')}_{n_x' n_z'}) = \delta_{nn'} \delta_{n_x n_x'} \delta_{n_z n_z'}.$$

The POD modes are optimal in the sense of capturing, on average, the most kinetic energy possible for a projection onto a given number of modes. Moreover each $\mathbf{\Phi}^{(n)}_{n_x n_z}$ inherits linear properties from the ensemble $\{\mathbf{u}^{(k)}\}$, such as incompressibility and boundary conditions.

In our application to plane Couette flow, we expand the perturbation velocity field $\mathbf{u}$ in terms of POD modes as

$$\mathbf{u}(\mathbf{x},t) = \sum_{n=1}^{\infty} \sum_{n_x=-\infty}^{\infty} \sum_{n_z=-\infty}^{\infty} a^{(n)}_{n_x n_z}(t) \mathbf{\Phi}^{(n)}_{n_x n_z}(\mathbf{x}), \quad (3.2)$$

where the amplitudes $a^{(n)}_{n_x n_z}$ are complex unless $n_x = n_z = 0$, in which case they are real. Translation symmetry in x and z implies optimality of the Fourier decomposition in these directions [4]:

$$\mathbf{\Phi}^{(n)}_{n_x n_z}(\mathbf{x}) = \frac{\boldsymbol{\phi}^{(n)}_{n_x n_z}(y)}{\sqrt{L_x L_z}} \exp\left(2\pi i \left(\frac{n_x x}{L_x} + \frac{n_z z}{L_z}\right)\right). \quad (3.3)$$

Ref. [5] describes how (3.1) can be reformulated as a matrix eigenvalue problem. Results using 4000 snapshots of the numerical data (expanded to $4 \times 4000 = 16000$ snapshots by symmetry operations, see [4, 5]) are given in Table 3.1. We note that most of the energy is contained in the $(n, n_x, n_z) = (1,0,0)$ mode, which represents the bulk of the turbulent modification of the mean flow. Fig. 3.1 shows the three most energetic POD modes.

Table 3.1: Eigenvalues of and percentage of average kinetic energy captured by the POD modes.

(n, n_x, n_z)	$\lambda^{(n)}_{n_x n_z}$	$\%E^{(n)}_{n_x n_z}$
$(1,0,0)$	4.4550	68.02
$(1,0,\pm1)$	0.7821	23.88
$(1,0,\pm2)$	0.0543	1.66
$(1,\pm1,0)$	0.0386	1.18
$(1,0,\pm3)$	0.0195	0.59
$(2,0,0)$	0.0174	0.27
$(2,0,\pm1)$	0.0123	0.38
$(1,\pm1,\pm2)$	0.0109	0.33
$(1,\pm1,\pm1)$	0.0090	0.27
$(3,0,0)$	0.0068	0.10
...		

4 Behavior of 11-Dimensional Model

We first consider the dynamics of an 11-dimensional model constructed by Galerkin projection of (1.1) onto the $(1,0,0)$, $(1,0,1)$, $(1,0,2)$, $(1,1,0)$, and $(1,1,\pm1)$ modes. (The behavior of the $(1,0,-1)$, $(1,0,-2)$, $(1,-1,0)$, and $(1,-1,\pm1)$ modes is thereby determined

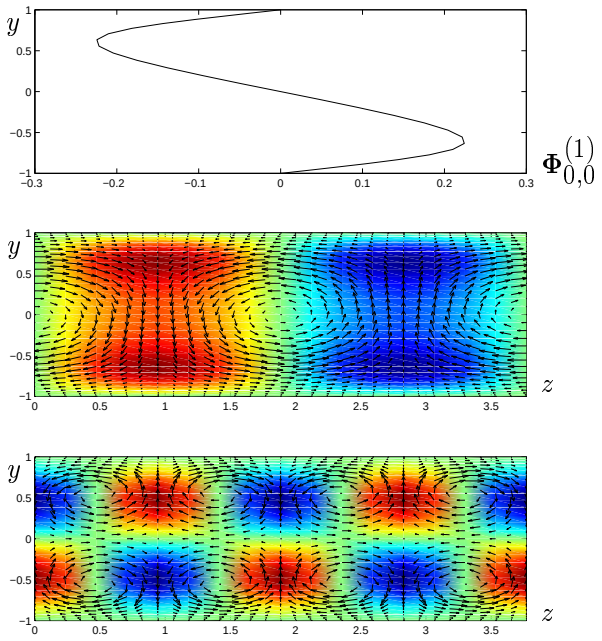

Figure 3.1: POD modes with $(n, n_x, n_z) = (1,0,0)$, $(1,0,1)$, and $(1,0,2)$. For the latter two, the vectors show the spanwise and wall normal components of the velocity, while the red (resp., blue) shading shows positive (resp., negative) streamwise velocity.

by complex conjugation, since $\mathbf{u}$ is real.) The equations for this model and more details are given elsewhere [9]. Integration of these equations reveals traveling wave behavior, with a solution of the form

$$a^{(n)}_{n_x n_z} = r^{(n)}_{n_x n_z} \exp(i(-\omega n_z t + \alpha^{(n)}_{n_x n_z})), \qquad (4.1)$$

where $\alpha^{(1)}_{00}$ is necessarily zero. Comparisons of the model behavior with that of the DNS projected onto the selected modes is given in Fig. 4.1. While the $(1,0,0)$, $(1,0,1)$ and $(1,0,2)$ modes reproduce the average energy budget rather well [9], the dynamical behavior of the model is unsatisfactory. The dynamics of the $(1,0,1)$ and $(1,0,2)$ modal coefficients obtained by projection of the DNS show the behavior to be roughly confined to a torus; each of these modes moves relatively quickly in and out along a radius in the plane, and drifts more slowly and chaotically around the circumference. The low-dimensional model we have described fails to reproduce the radial motion, and caricatures the circumferential motion as a simple traveling wave. Velocity field reconstructions of these traveling waves are not given here, but a little thought reveals that they would illustrate a simple translation of streak/vortex structures in the spanwise direction. Indeed, this model completely fails to capture the streak breakdown and regeneration process, as the

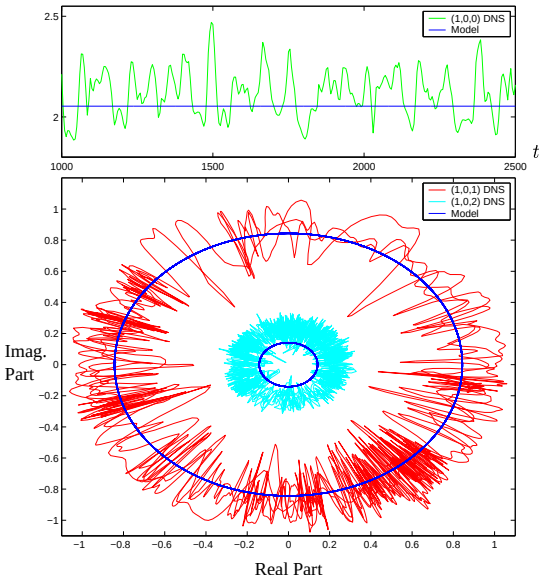

Figure 4.1: Behavior of the 11-dimensional model without modeling losses to neglected modes.

RMS modal velocities remain constant in time [9].

5 Improvements to the 11-Dimensional Model

Here we improve the 11-dimensional model considered in the previous section by including terms which model losses to modes which have been neglected in our truncation. The simplest model for such losses is a spectral eddy viscosity model (cf. [4]), where terms of the form

$$-\alpha\nu(n_x^2 + n_z^2)a^{(n)}_{n_x n_z}$$

are added to the equation for the evolution of $a^{(n)}_{n_x n_z}$. The effectiveness of the spectral eddy viscosity model is tested by numerically calculating the magnitude of the neglected terms; a least squares fit between the numerically calculated terms and those that result from application of the model gives $\nu = 0.0333$. We then "tune" the $\mathcal{O}(1)$ parameter α to get a good fit between the behavior of the model and the DNS.

The bifurcation diagram of Fig. 5.1 shows existence and stability of solutions as a function of α. As α is increased from zero, we encounter several solution types: the previously described traveling waves (denoted TW), two different types of standing waves (SW_1 and SW_2) and modulated traveling waves (denoted MW). Diagrams of the behavior of the $(1,0,1)$ and $(1,0,2)$ modal amplitudes for these solutions are shown at the bottom of Fig. 5.1. All solutions with the exception of the MW are stable over some interval of α.

We note that the SW_2 solution, for which the

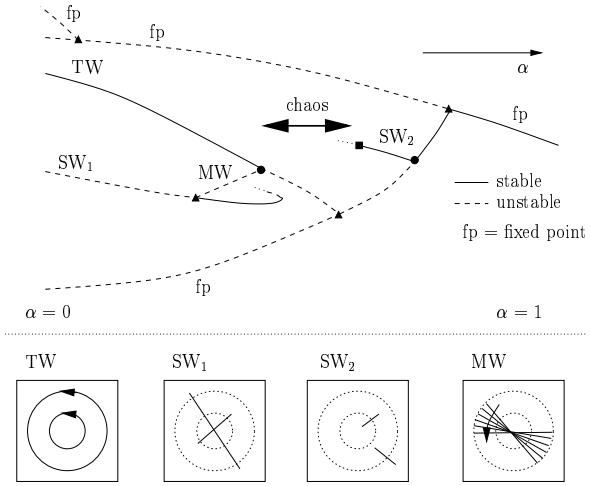

Figure 5.1: (Top) Schematic bifurcation diagram with respect to α. (Bottom) Projections as in Fig. 4.1 of the $(1,0,1)$ and $(1,0,2)$ modal amplitudes for the solutions.

$(1,0,1)$ and $(1,0,2)$ modal amplitudes oscillate along radii, captures the most interesting DNS dynamics, namely the streak breakdown and regeneration process. When $\alpha = 0.8$ we obtain the dynamics of the RMS modal velocities illustrated in Fig. 5.2; this solution also gives reasonable velocity field reconstructions: see Fig. 5.3. The model's turbulence statistics also exhibit the same qualitative forms as those of the DNS [9].

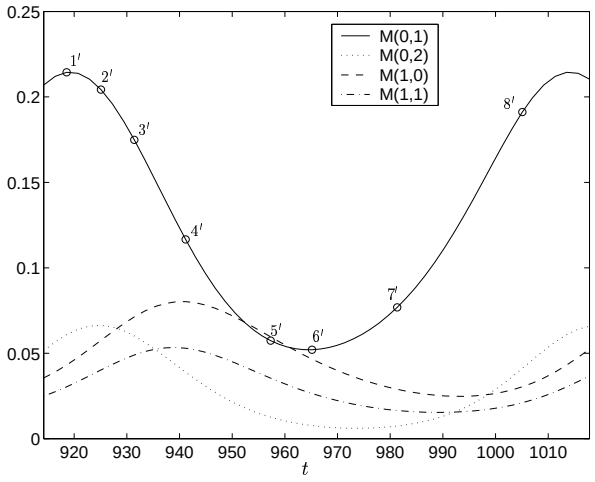

Figure 5.2: RMS modal velocity for 11-dimensional model with modeling of losses to neglected modes ($\alpha = 0.8$).

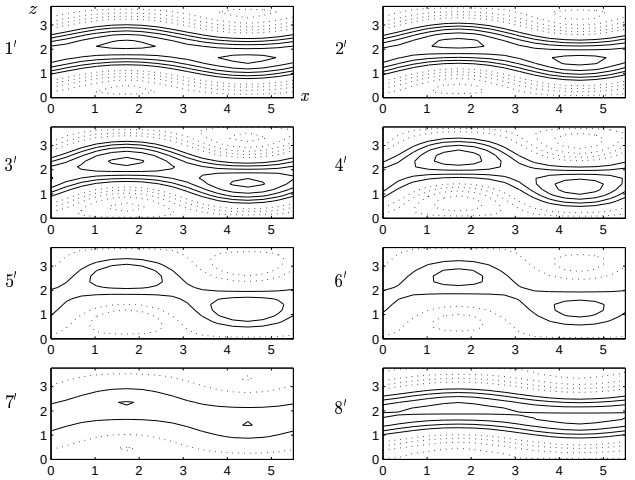

Figure 5.3: Midplane streamwise-velocity contours for the 11-dimensional model with modeling of losses to neglected modes ($\alpha = 0.8$).

6 Control Using the Phase Response Curve

A phase response curve (PRC) describes the phase-shift of an oscillation as a function of the phase of a stimulus or impulsive perturbation [10]. For the present problem, suppose that the speed U_0 of the parallel plates is very briefly changed. This perturbation will have the largest effect on the turbulent mean flow, which is captured in our model by the amplitude $a_{00}^{(1)}$. We thus consider how the timing of an instantaneous perturbation $a_{00}^{(1)} \to a_{00}^{(1)} + \Delta a$ affects the time at which subsequent streak breakdowns occur.

We define $\theta = 0$ to be the phase of the periodic orbit at which $\mathrm{M}(1,0)$ is minimal, i.e., before streak breakdown. The phase θ is a simple parametrization of time, evolving according to $\dot{\theta} = 2\pi/T$, where T is the period of the periodic orbit. Thus, at $\theta = 2\pi$ the periodic orbit has returned to the state at which $\mathrm{M}(1,0)$ is minimal. Let $\Delta\theta$ be the change in phase associated with the perturbation Δa. A positive (resp., negative) $\Delta\theta$ means that the next streak breakdown occurs before (resp., after) its unperturbed occurrence. We calculate

$$\frac{\partial \theta}{\partial a} = \lim_{\Delta a \to 0} \frac{\Delta \theta}{\Delta a} \tag{6.1}$$

by solving the appropriate adjoint problem with the software XPPAUT [11]. The phase parametrization of the periodic orbit and the PRC are shown in Figure 6.1; note that the abscissa for the PRC plot represents the phase at which the perturbation is applied. We see that the perturbation can either advance or retard the time at which the subsequent streak breakdowns occur. Figure 6.2 illustrates that, to delay the subsequent streak breakdowns, our model predicts that it is best

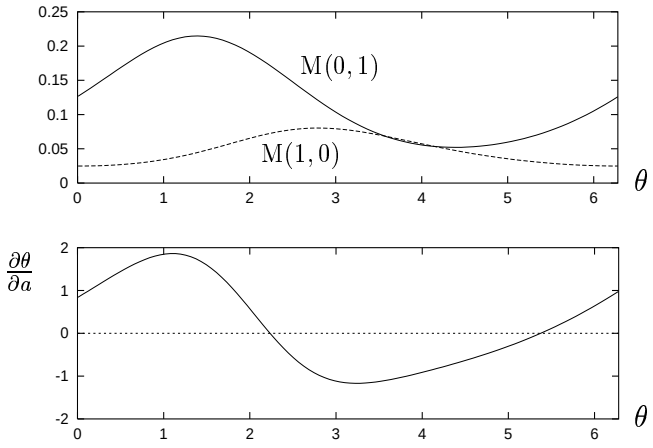

Figure 6.1: (Top) One periodic cycle for our phase parametrization. (Bottom) The phase response curve for perturbations as described in the text.

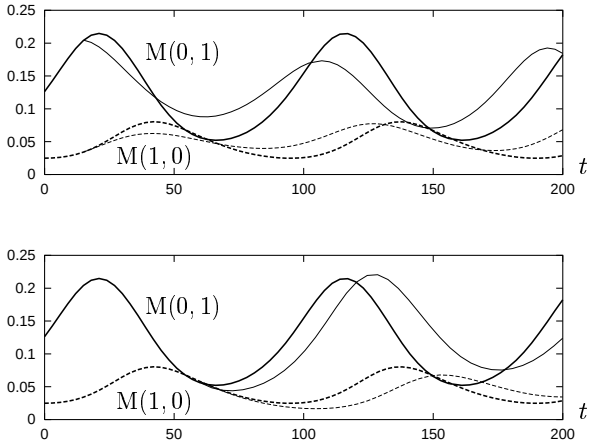

Figure 6.2: Solid (resp., dashed) lines show M(0, 1) (resp., M(1, 0)), with thick (resp., thin) lines corresponding to the unperturbed (resp., perturbed) case. The perturbation is $\Delta a = 0.5$ at (top) $\theta = 1$, corresponding to $t = 15.11$, and (bottom) $\theta = 4$, corresponding to $t = 60.45$.

to apply the perturbation just after the current streak breakdown; for clarity, a relatively large perturbation $\Delta a = 0.5$ to the $\mathcal{O}(1)$ quantity $a_{00}^{(1)}$ has been used for this figure. Comparison with full simulations of the perturbed flow are in progress.

7 Conclusion

We have modeled turbulent plane Couette flow for a Minimal Flow Unit (the smallest domain in which turbulence can be sustained) by expanding the velocity field as a sum of optimal modes calculated via the proper orthogonal decomposition from numerical data. Ordinary differential equations were obtained by Galerkin projection of the Navier-Stokes equations onto these modes. We found that a 6 mode (11-dimensional) model, with additional modeling of neglected modes, nicely captures the streak breakdown and regeneration process as a periodic orbit. We then calculated the phase response curve for this periodic orbit for an impulsive perturbation to the mean flow. Depending on its timing, such a perturbation can either advance or retard the time at which subsequent streak breakdowns occur; this suggests how streak breakdown can be controlled through appropriately timed perturbations.

References

[1] P.G. Drazin and W.H. Reid, *Hydrodynamic Stability* (Cambridge University Press, Cambridge, 1981).

[2] O. Dauchot and F. Daviaud, "Finite amplitude perturbation and spots growth mechanism in plane Couette flow," Phys. Fluids **7**, 335 (1995).

[3] J. Hamilton, J. Kim, and F. Waleffe, "Regeneration mechanisms of near-wall turbulence structures," J. Fluid Mech. **287**, 317 (1995).

[4] P. Holmes, J.L. Lumley, and G. Berkooz, *Turbulence, Coherent Structures, Dynamical Systems and Symmetry* (Cambridge University Press, Cambridge, 1996).

[5] J. Moehlis, T.R. Smith, P.J. Holmes, and H. Faisst "Models for turbulent plane Couette flow using the proper orthogonal decomposition," Phys. Fluids **14**, 2493 (2002).

[6] B. Podvin and J. Lumley, "Low-dimensional approach for the minimal flow unit," J. Fluid Mech. **362**, 121 (1998).

[7] F. Waleffe, "On a self-sustaining process in shear flows," Phys. Fluids **9**, 883 (1997).

[8] B. Eckhardt and A. Mersmann, "Transition to turbulence in a shear flow," Phys. Rev. E **60**, 509 (1999).

[9] T.R. Smith, PhD Dissertation, Princeton University, 2003.

[10] A.T. Winfree, *The Geometry of Biological Time* (Springer-Verlag, New York, 2001).

[11] B. Ermentrout, *Simulating, Analyzing, and Animating Dynamical Systems: A Guide to XPPAUT for Researchers and Students* (SIAM, Philadelphia, 2002).